In situ studies of growth of carbon nanotubes on a local metal microheater

Cite as:
Nerushev, O.A., Ek-Weis, J. & Campbell, E.E.B. (2015). In situ Studies of Growth of Carbon Nanotubes on a Local Metal Micro-Heater, 26(50), [505601].

Manuscript received: 22/06/2015; Accepted: 22/10/2015; Article published: 18/11/2015

In situ Studies of Growth of Carbon Nanotubes on a Local Metal Micro-Heater

O.A. Nerushev[1], J. Ek-Weis[1*], E.E.B. Campbell[1,2]

1: EaStCHEM and School of Chemistry, University of Edinburgh, David Brewster Road, Edinburgh EH9 3FJ, Scotland.

2: Division of Quantum Phases and Devices, School of Physics, Konkuk University, 143-701, Seoul, Korea

Abstract

Using electron microscopy and *in situ* Raman spectroscopy we investigate carbon nanotube growth from ethylene on iron catalyst islands patterned on top of Mo electrodes, using a highly localized resistive on-chip-heating technique. A clear transition is observed between multi-walled and single-walled nanotube growth as the local temperature of the heater is increased. This can be rationalized in terms of the balance between incoming carbon flux and diffusion through the catalyst particle. The observed changes in heater performance on exposure to the hydrocarbon gas are explored and related to the formation of molybdenum carbide, leading to a rapid change in resistivity and heating power that increases the local temperature of the heater by up to 100 ^{o}C. This provides optimum conditions for nanotube growth after an incubation time that depends on the carbon flux.

* Current address: J. Heyrovsky Institute of Physical Chemistry, Academy of Sciences of the Czech republic, v.v.i., Dolejskova 3, CZ-18223 Prague 8, Czech Republic

1. Introduction

Microscale heaters have been used in recent years in order to demonstrate and study the growth of carbon nanotubes and nanowires.[1-11] The advantages of such an approach are two-fold. Firstly, the small thermal mass of the heater provides a means of rapidly controlling and varying the growth conditions and secondly, the technique provides a means of locally growing carbon nanotubes and nanowires on substrates that would not survive the conditions of a conventional CVD growth chamber. The studies have typically employed suspended polysilicon heaters[1, 3, 6, 7, 10, 11] with the most recent work looking at the temperature dependence of the maximum height reached by vertically-aligned multi-walled nanotube films [10]. Other approaches have incorporated microheaters on the back side of substrates [3] or embedded in suspended membranes [5]. Although these approaches provide a reliable and practical temperature determination via the measurement of the heater resistance, important for controlling the growth behaviour, the fabrication can be complex. We have followed a slightly different approach in the use of simple metallic microheaters, patterned directly on silicon chips, that can be easily fabricated using standard lithography [2, 8, 9, 12]. These have the advantages of simplicity and a direct means of electrically contacting the grown structures but the disadvantage of complicating the temperature determination since the properties of the heater change on exposure to hydrocarbon gas at elevated temperatures [12]. In this paper we use metal microheaters to investigate carbon nanotube growth using iron catalyst particles and ethylene as hydrocarbon feedstock. We also explore the reasons behind the rapid change in heater properties on exposure to the hydrocarbon gas.

In situ measurements, important for understanding growth kinetics, have been performed in recent years for laser vaporisation growth [13],[14], cold wall chemical vapour deposition (CVD) [15],[16] real-time surface XPS [17], mass spectrometry of ethylene conversion[18], microbalance studies [19] and plasma-enhanced CVD growth of nanotubes and nanofibres [20],[21] to achieve a more detailed understanding by observing the tubes or their environment directly during growth. The use of the local microheater technique allows us to combine a small heater chamber with a conventional micro-Raman spectrometer and optical microscopy for CNT growth visualisation [9], [12]. Previously, *in situ* Raman spectroscopy was

performed with conventional oven CVD growth [22] [23] for direct measurements of the evolution of the G-peak intensity with growth time and correspondingly, an estimation of the initial growth rate and timescale for catalyst degradation. Previously we have used [9] micro-Raman spectroscopy in combination with local-heater growth for measurement of the time evolution of the G to D peak ratio and the broadening of Raman spectra in the vicinity of the radial breathing mode (RBM) vibrations for investigation of CNT quality and diameter distribution in the early stage of growth. In the present work we have improved the time resolution of the Raman imaging and we follow the development of growth as a function of temperature showing the sharp transition from multi-walled growth at low temperature to single-walled growth at higher temperatures and the onset of catalyst poisoning for high temperatures and high carbon flux. The *in situ* Raman spectroscopy studies are combined and compared with *ex situ* Raman spectroscopy and electron microscopy. The results are in very good qualitative agreement with the predictions of a growth model formulated by Woods et al. to explain the results of *in situ* studies of conventional CVD growth of multi-walled nanotube arrays using acetylene as the hydrocarbon feedstock. [14]

2. Experimental

Carbon nanotubes were grown using a local heating technique, which has been described in more detail elsewhere [8, 9, 12]. A small molybdenum strip was deposited on a silicon chip and connected to four large contact pads (figure 1). This functions as a resistive heater and the configuration with four contacts allows the voltage drop across the heater to be monitored as a function of the applied current and time, thus monitoring changes in the heater resistivity and applied power. Rectangular catalyst islands of 1 nm thick Fe supported by 5 nm of Al_2O_3 were deposited on top of this strip. All chips in the present work were fabricated on the same Si wafer with identical design and fabrication procedure that provided good reproducibility and the possibility to compare directly the influence of experimental conditions. Some experiments were performed on iron-free chips to study the influence of the growth conditions on the Mo heater and how it changed during heating and gas exposure. Heating occurred by passing an electrical current through the Mo strip. The current was provided by a precision Keithley source-meter controlled with a LabView program, which simultaneously monitored the voltage drop across the heater. The chip containing the heater was placed in a small custom-built vacuum chamber that

was connected up to gas supplies and placed inside a Renishaw micro-Raman spectrometer.

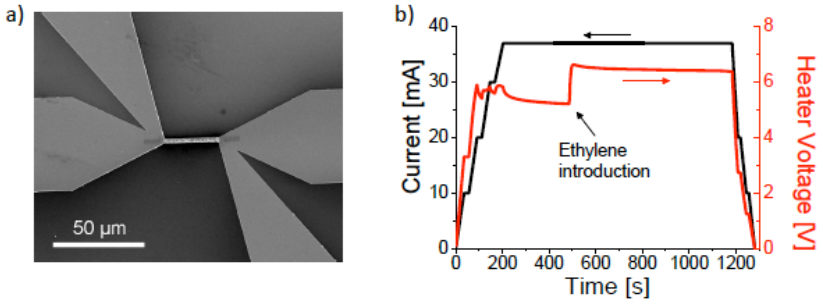

Figure 1. a) Heater with 4 electrodes connected to contact pads; b) Typical applied heater current (black) and corresponding voltage drop (red) across the heater during a growth run.

A constant flow of 300 sccm hydrogen and 500 sccm argon was supplied during the whole process. Ethylene, introduced downstream of the carrier gases, was used as carbon feedstock and the flow rate was varied between 6 and 100 sccm (6, 12, 30, 100 sccm). The gas was supplied via a 2m long Swagelok tube with an inner diameter of 3mm (internal volume 15 cm^3). The delay time for the gas to reach the growth chamber was 2s, this value was subtracted from all time-dependent plots. The feedstock gas was introduced to the system after the heater current reached the desired value. The current was gradually increased in a few steps to allow gentle annealing of the catalyst and heater body. Since the heater was deposited via electron beam evaporation of molybdenum onto the silicon chip under room temperature conditions, the resistivity of the Mo layer is larger than that of the bulk metal and gradual annealing and reduction in the H_2 atmosphere results in a decrease of the heater resistivity. This can be seen in Fig 1(b) as a decrease in the voltage drop across the heater with time for each current step. The carbon feedstock was introduced to the growth chamber only after a stable voltage drop across the heater was reached for a given current. The introduction of the hydrocarbon gas is accompanied by a noticeable jump in the voltage drop, indicating a higher resistivity and correspondingly greater heating power [12]. The working current through the heater was varied in the range 36-42 mA, which resulted in initial temperatures (immediately prior to hydrocarbon injection) from 630 °C to 690 °C. The temperature was determined from analysis of the grey-body radiation from the heater [9, 12] using the same spectrometer which was used for Raman spectra acquisition. Previous studies

showed that the temperature increase on introduction of the hydrocarbon gas was typically ca. 90 ^{o}C.[12] A relatively short laser excitation wavelength of 514 nm was used for the Raman measurements in order to minimise the background from the heater radiation and we therefore did not directly evaluate the temperature during the *in situ* time-dependent growth studies. The Raman laser intensity was kept sufficiently low to avoid any influence on the growth through additional heating of the underlying substrate. Each Raman spectrum was accumulated for 15 seconds to provide the best compromise between time resolution and signal/noise.

3. Results

3.1. Transition from multi-walled to single-walled nanotube growth

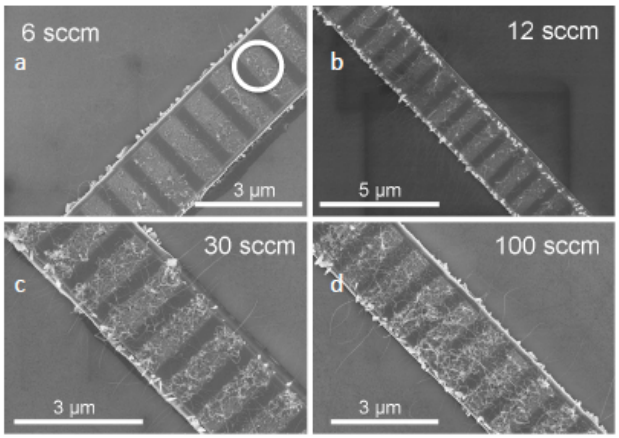

Figure 2. SEM images of nanotubes grown at a heater current of 37 mA, corresponding to an initial heater temperature of 640 °C, for different ethylene flow rates, as indicated on the images and a growth time of (a) 900s, (b) 800s (c), (d) 700 s. White circle on first image shows the Raman laser probe size.

Examples of CNT grown under different ethylene partial pressures with fixed initial heater temperature are shown in figure 2. Note, that as shown previously [9, 12] and discussed later, the temperature of the heater increases once the carbon feedstock has been introduced to the growth chamber and the actual growth temperature, for the conditions in Figure 2, is on the order of 700-750^{o}C. The initial heater temperature in the present studies is lower than in our earlier investigation of single-walled nanotube growth [9] due to the different geometry of the Mo heater and the age of the heaters. What is critical for growth is the temperature that is reached for a given heater current after the carbon feedstock has been introduced, this depends on the annealing process

that the heater has undergone and the changes to the heater that occur on exposure to the hydrocarbon gas. In the present series of measurements the heaters were all produced in the same batch and should behave identically on heating. The reproducible correlation between the current and the initial temperature determined spectroscopically provides confidence that this is so. Although the nanotubes in the present series of experiments are generally not well aligned due to the turbulent nature of the gas flow around the growth zone, we have shown previously that a high degree of alignment can be achieved by applying an external electric field during growth.[8]

Figure 2 shows a visible increase in the amount of nanotubes covering the surface with increased partial pressure of the carbon feedstock gas. Under these conditions the nanotubes are predominantly single-walled nanotubes as confirmed by Raman measurements discussed below. The lighter structures at the cooler edge of the heater are small bundles of multi-walled nanotubes that are also seen to grow under the lowest temperature/heater current investigated and particularly for high ethylene partial pressures [8]. The SEM image in Figure 3 shows the growth product at the lowest heater temperature investigated and with a high ethylene flow rate (30 sccm). In addition to the bundles of small multi-walled nanotubes that are grown, it is possible to see the deposition of amorphous carbon on the material irradiated by the laser beam. This was only observed for high partial pressures of feedstock when bundles of multi-walled carbon nanotubes were grown, with the deposition occurring on the nanotubes heated by the laser. SEM images for other growth conditions are shown in the Supplementary Information.

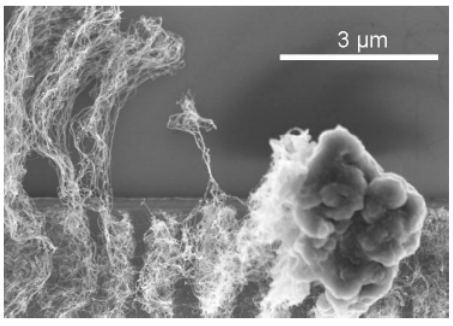

Figure 3. SEM image of bundles of multi-walled carbon nanotubes grown for low heater current/temperature (36 mA, initial temperature 630 ^{o}C) and high ethylene partial pressure (30 sccm). A significant amount of amorphous carbon was deposited on the nanotubes within the Raman laser spot only for these conditions of high ethylene partial pressure and multi-walled carbon nanotube growth, with no visible deposition outside this area.

In order to visualise the abrupt changeover from multi-walled to single-walled nanotube growth, a tapered heater was fabricated with a temperature gradient along its length. The results are shown in Figure 4. The heater temperature *during growth*, as estimated from analysing the grey body radiation [12], is indicated on the x-axis. The corresponding Raman spectra recorded after growth are shown in Figure 5(a). Vertically-aligned multi-walled nanotubes are seen to grow at the lower temperature end of the heater (visible due to the higher scattering contrast) in Figure 4 within a narrow temperature range of ca. 670 – 700 ^{o}C. This can also be clearly seen in the series of Raman spectra in Figure 5(a) where the transition from a broad G-peak and large D-peak, typical of multi-walled nanotubes, to a narrow G peak and very small D peak more typical of single-walled nanotubes is seen to occur at around 700-720 ^{o}C. In this temperature range both single- and multiwalled nanotubes are present as can be seen in the SEM picture (Fig 4) where single-walled nanotubes can be seen extending outwards from the edges of the heater while the multi-walled nanotubes grow in vertical bundles. A plot of the ratio of the integrated G and D peaks in Figure 5(b) shows that the optimum G/D ratio, indicating the best quality single-walled nanotubes is achieved for a heater temperature of 730-740 ^{o}C.

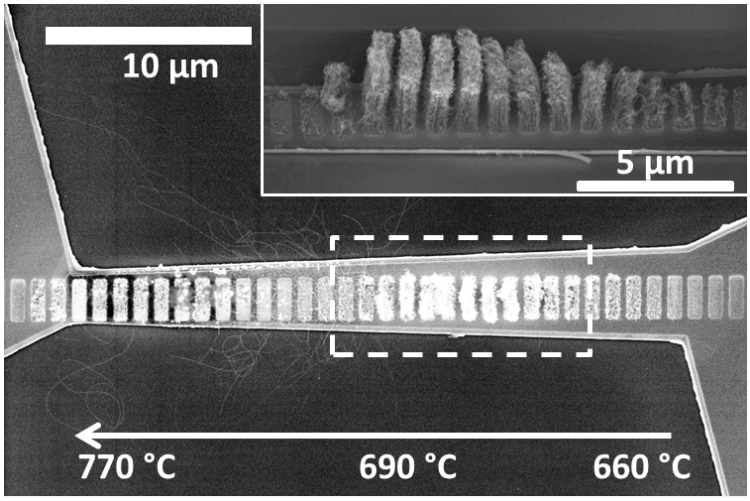

Figure 4. Nanotubes grown on a heater with the right hand side 4 µm wide and the left hand side 2 µm wide. In this case, the heater temperature was monitored during growth and ranged from 660 ^{o}C (right) to 770 ^{o}C (left). Vertically-aligned multiwalled nanotubes have a higher scattering intensity in the SEM and are clearly visible at heater positions corresponding to ca. 670 -700 ^{o}C. Note that the transition to multi-walled nanotube growth can also be seen at the far left hand side of Figure 4 where the temperature abruptly decreases.

The abrupt change from multi-walled nanotube growth to single-walled nanotube growth as the temperature is increased was predicted by Wood et al. [24] with a model that was developed to explain the results of *in situ* studies of conventional CVD growth of muti-walled nanotube arrays using acetylene as the hydrocarbon feedstock. [14] The model considers the single-walled nanotube growth rate as a function of incoming carbon flux and the role of poisoning at high temperatures that reduces the amount of atomic carbon that enters the catalyst particle. The optimum growth temperature for single-walled nanotubes modelled for C_2H_2 decomposition on an iron catalyst was found to be ca.700 ^{o}C. For temperatures below this value the incoming carbon flux for single-walled nanotube growth exceeds the diffusion flux through the catalyst particle and therefore multi-walled nanotubes preferentially form. For temperatures above 700 ^{o}C, the so-called high temperature regime, not enough carbon is supplied at the optimum growth rate for these temperatures, therefore the number of walls rapidly decreases, leading predominantly to single-walled nanotube growth. Additionally, the high carbon flux leads to rapid onset of poisoning of the catalyst and cessation of growth due to the formation of a coating on the catalyst surface [25]. The optimum temperature was found to be largely independent of the incoming flux of hydrocarbon. The results for the local heater growth are in exceptionally good agreement with the predictions of this relatively simple model. The catalyst system used is similar (Fe), however, the use of ethylene as precursor leads to a much slower growth than is the case for acetylene and the transition in growth behaviour is more clearly delineated than in the original macroscopic acetylene growth study [14]. The difference in growth behaviour from ethylene and acetylene precursors is well known and can be predominantly attributed to their different thermodynamic stabilities.[26] The conditions of growth for the local heater experiments tend to accentuate the difference since there is no significant pre-heating of the precursor gas before the molecules reach the Fe catalyst.

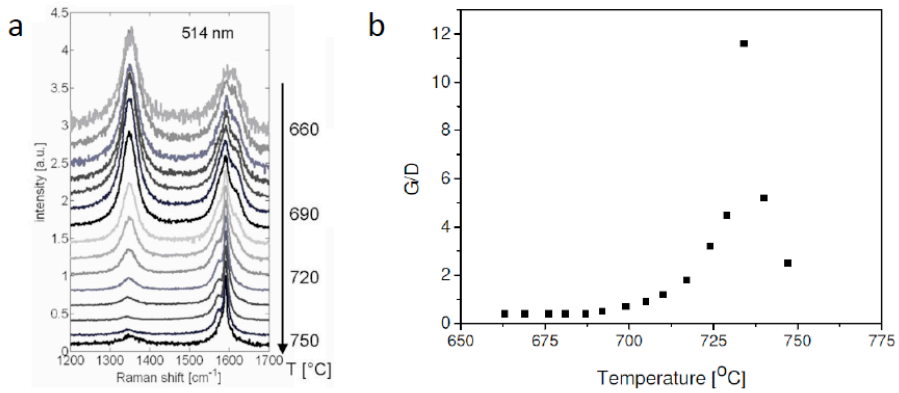

Figure 5. a) Raman spectra in the D-G region along the heater shown in Figure 4. The spectra were obtained after growth using a laser wavelength of 514 nm and power density of 0.1 mW/μm^2. All spectra are normalised to the height of the G-peak and are shifted vertically for clarity. b) Ratio of the integrated G and D peak intensities from the spectra in Fig. 5(a), showing the maximum ratio at an estimated growth temperature of ca. 730 – 740 ^{o}C.

3.2. *In situ* Raman studies: growth kinetics

In order to follow the growth kinetics under different growth conditions, we use *in situ* Raman spectroscopy. A comparison of the Raman spectral intensity allows a quantitative comparison of growth rate under different conditions. These experiments were carried out using the heater arrangement shown in Figure 1. The white circle in Fig 2(a) indicates the size of the laser focus.

The evolution of the Raman spectra in the D-G region for nanotubes grown using 30 sccm ethylene at 37 mA (initial temperature of 640 °C, growth temperature ca. 730 ^{o}C) is shown in Figure 6 (corresponding to the image in Figure 1c). The intensity of the G peak first rapidly increases and then levels off. There is practically no signal in the region of the D peak (~1300 cm^{-1}), which indicates that that the growing nanotubes are single-walled nanotubes with few defects and with no detectable deposition of amorphous carbon for these growth conditions.

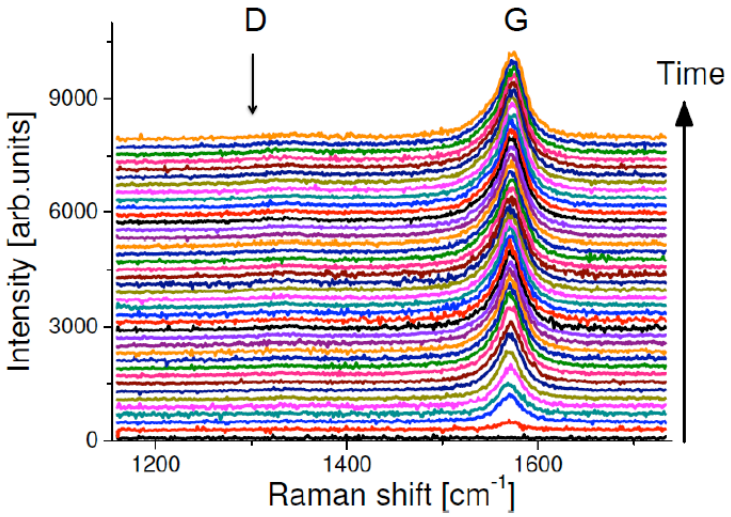

Figure 6. Series of Raman spectra obtained during growth of CNT with 30 sccm C_2H_4 and an initial heater temperature of 640 ^{o}C over a time period of ca. 10 minutes.

Figure 7(a) shows the time evolution of the integrated area of the G peak as a function of time for different initial heater current/temperatures with a fixed ethylene flow rate of 30 sccm, whereas Figure 7(b) shows the time evolution for nanotubes grown with the same heater current (37mA, initial temperature 640 °C, growth temperature ca. 730 ^{o}C) and varying flow rates of ethylene. Further data series are available in the Supplementary Information. Time 0 s is defined to be when the ethylene flow reached the growth chamber and the first Raman measurement was started.

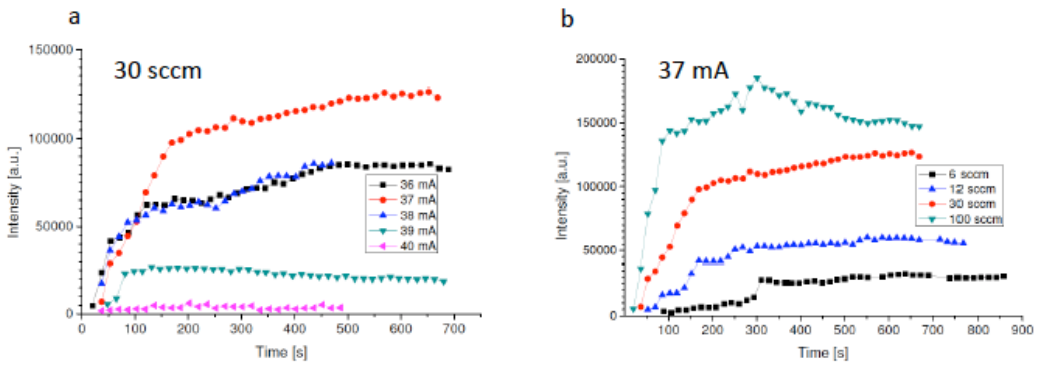

Figure 7. Time dependence of the integrated Raman G-peak for a) fixed ethylene flux (30 sccm) and b) fixed heater current (corresponding to an initial heater temperature of 640 ^{o}C, growth temperature of ca. 730 ^{o}C).

The intensity of the G peak first rapidly increases and thereafter follows a slower linear growth rate followed by a saturation in the growth rate, most apparent for the highest temperatures investigated, that can be related to the catalyst poisoning, as discussed above. The initial fast increase in Raman signal mirrors the time-dependence of the nucleation of nanotubes and is in agreement with earlier experiments that showed an increasing range of SWNT diameters in the Raman spectra as the growth time increased over a time range of 10 minutes with smaller diameter nanotubes developing first.[9] A similar broadening of the diameter distribution with increasing time and carbon flux was also observed under very different growth conditions [27], [28]. In some cases in Fig 7 and in the data shown in the Supplementary Information, a small decrease in signal is detected. This decrease can be due to either a small drift of the laser spot to a location with fewer nanotubes or due to growing nanotubes falling out of the laser spot or falling down on the surface. This would reduce the Raman signal since the nanotubes that are suspended during growth would be expected to yield a stronger Raman signal [29]. The larger drop that is sometimes observed for 100 sccm C_2H_4, visible in Figure 7(b), may be attributed to the laser burning of amorphous carbon that can be seen to be deposited on laser heated nanotubes for high flow rate conditions (Fig. 3). A similar trend of a decreasing signal with time in conventional CVD *in situ* growth studies was measured by laser absorbance in [30], where it was attributed to burning of the nanotubes due to air leaking into the chamber, however, since we only observe the decrease in intensity for high carbon flux conditions this is unlikely to be the reason.

Figure 7(a) shows a non-monotonic Raman signal dependence on heater current/temperature for fixed ethylene partial pressure. The Raman signal first increases as the heater current is increased and then decreases again. The increase in Raman signal on increasing the heater current from 36 mA to 37 mA is related to the change from multi-walled to single-walled nanotube growth, as discussed above. The G-peak intensity is much stronger for the single-walled nanotubes. The decrease in intensity on moving to higher heater currents can be related both to a change in density of suitable catalyst particles and to the more rapid onset of poisoning for the higher temperature conditions, with the fastest growing, smallest diameter single-walled nanotubes being stopped preferentially, in qualitative agreement with the predictions of the Wood et al. model [24]. Additionally, a coarsening of the active

nanoparticles may occur at the higher temperatures due to increased mobility on the surface also contributing to a decrease in the single-walled nanotube signal due to a decreasing density of suitable catalyst particles. To explain the initial rapid increase in signal we can consider that the catalyst films transform to an ensemble of nanoparticles with a very broad size distribution[31] during the annealing stage. These nanoparticles serve as the catalysts for ethylene decomposition and simultaneously dissolve the carbon. During an incubation period there can be changes to the size distribution and morphology of the particles before the growth of nanotubes occurs [32] that can be due to the increased content of dissolved carbon and/or a local temperature rise due to the exothermic nature of the ethylene decomposition.

In contrast to the temperature dependence of the Raman signal, the hydrocarbon flux dependence is monotonic and shows the intuitively expected increase in the Raman signal with increasing flux of carbon feedstock (Figure 7(b)) for any given temperature. Both the initial fast growth rate, with increasing extent of nucleation with time, and the slower "steady-state" growth rate increase with increasing carbon flux for the results shown in Fig.7(b). The general trend of the growth results is very similar to what has been found previously in *in situ* measurements of bulk growth in conventional CVD set-ups such as an inverse relationship between the initial growth rate and the lifetime of the catalyst particles [30, 33, 34].

In addition to the different Raman scattering intensities, Figure 7(b) also shows a flux-dependent time delay between the injection of the carbon feedstock and the appearance of a detectable Raman signal. This will be addressed in the following section.

3.3 Time-dependent properties of the heater

A typical current-voltage behaviour of a heater is shown in Fig. 1(b). Analysis of voltage and current logs shows that the voltage drop over the heater is not constant and changes non-monotonically in time, reaching a maximum voltage for a certain time delay. The amplitude of the change in voltage drop and the characteristic times involved depend on the ethylene flow rate. This is shown in Fig. 8.

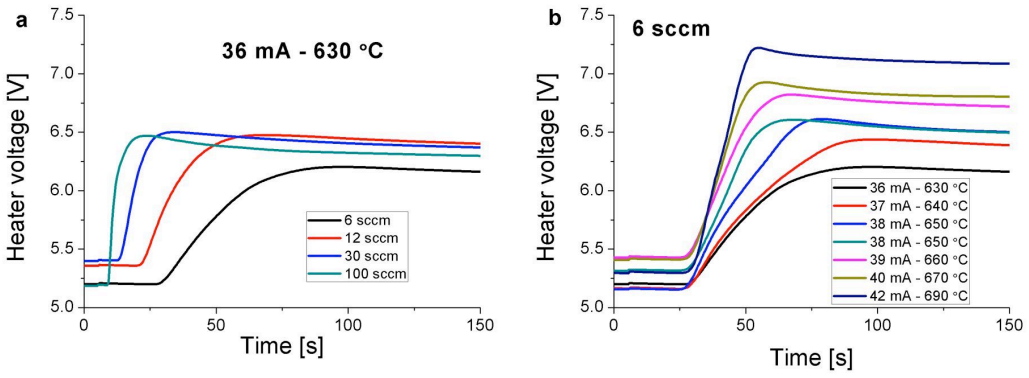

Figure 8. Heater voltage drop versus time for: a) fixed heater current of 36 mA and b) fixed ethylene flow rate of 6 sccm. Zero time corresponds to ethylene injection.

Directly after ethylene injection the heater resistivity remains at a constant level for a certain "incubation time" and then rapidly grows by 30-40%, reaches a maximum value and then slowly decreases by a few %.

The incubation time does not depend on the initial heater current/temperature within the investigated range but only on the carbon feedstock partial pressure, as seen from a comparison of figures 8(a) and 8(b). All data on the measured incubation time may be summarised on a single ln-ln plot of the incubation time versus the ethylene partial pressure (figure 9(a)), showing that it is the amount of carbon that the heater is exposed to that is the critical parameter within the relatively narrow initial heater temperature range of interest.

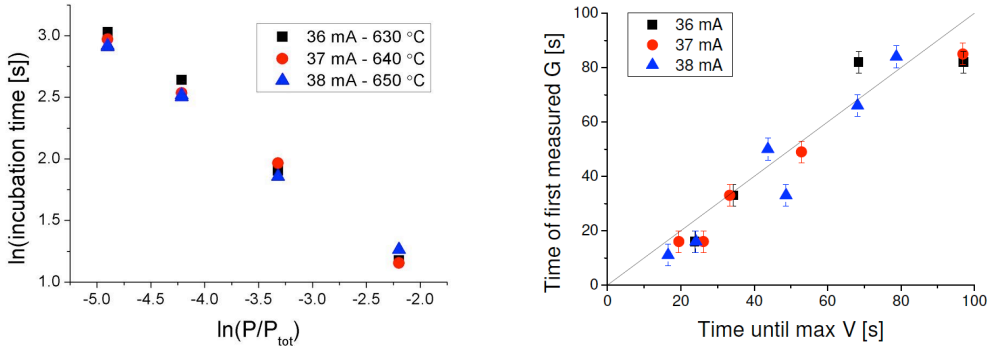

Figure 9. a) Correlation between partial ethylene pressure and initiation time for different initial heater temperatures. The "dead time" needed for the gas to travel from the mass-flow controller to the reactor chamber has been subtracted from the raw data. b) Plot of the time after exposure to ethylene before a signal is detected in the G-band region of the Raman spectrum versus the time needed for the voltage drop across the heater to reach its maximum value. The straight line indicates equal times.

There is a delay in the appearance of the Raman signal (even accounting for the time it takes for the ethylene to reach the substrate), visible in Fig. 7(b). In Figure 9(b), this delay is plotted against the time it takes for the voltage drop across the heater to reach its maximum value. Vertical error bars correspond to the acquisition time for a single Raman spectrum that defines the best achievable time resolution on this axis. A very good correlation between these delay times was observed which confirms that changes in the heater resistivity (as reflected in the measured voltage drop) are closely related to the onset of nanotube growth.

The maximum voltage drop across the heater indicates the maximum resistivity and hence maximum heating power corresponding to an increase in heater temperature of up to 100 ^{o}C [12]. An image of a heater before and after ethylene introduction is shown in the Supplementary Information and a very noticeable increase in the brightness of thermal radiation can be clearly seen. It is this rapid increase in temperature that is responsible for initiating the nanotube growth. We now address the reasons for this sudden increase in voltage drop and corresponding heater temperature.

A set of control experiments was performed on catalyst-free heaters exposed to ethylene (the alumina layer was present as in the heaters used for nanotube growth, the only difference was the missing iron deposition). A similar rapid change in voltage drop and hence resistivity of the heater was observed after the appropriate time delay. Raman spectroscopy was carried out *ex situ* on these heaters after ethylene exposure, allowing the collection of spectra with much higher accumulation time than used for the nanotube growth experiments (600 s compared to 15 s). The results are shown in Figure 10.

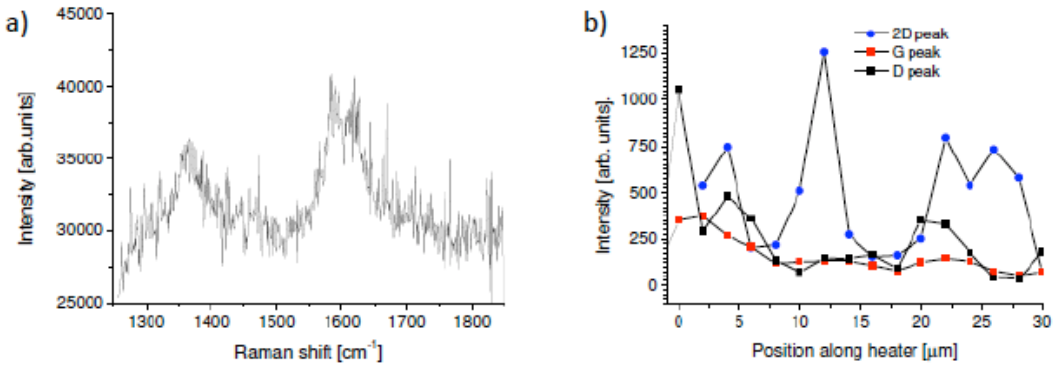

Fig.10. Raman signal on catalyst-free sample after exposure to ethylene. a) typical Raman signal in D-G spectral range (accumulation time 600 s), b) G, D, 2D peaks signal profile along the heater.

A small signal intensity is seen that can be attributed to graphene formation on top of the Mo heater. Note that this signal is so weak that it will not contribute to the spectra collected *in situ* during growth with a much shorter accumulation time. The intensity of the 2D peak fluctuates significantly along the heater. The relative intensity of this peak is known to be strongly dependent on the number of graphene layers (with the highest 2D/G ratio corresponding to single layer graphene).

The presence of graphene layers on top of the heater provides evidence for the conversion of the molybdenum heater to molybdenum carbide on exposure to the hydrocarbon. Molybdenum carbide is known to be a catalyst for graphene formation [35]. The resistivity of molybdenum carbide is also significantly higher than that of molybdenum thus the conversion to carbide on exposure to the hydrocarbon gas provides the mechanism for the large step change in the voltage drop reflecting the change in resistivity (Fig. 1(b)) and resulting in a significantly higher heater temperature. The delay in voltage step change can be considered to be related to the time it takes for the carbide formation at the grain boundaries to develop to such an extent that it will disrupt the conductivity through the Mo layer. The resistivity change will continue until the conversion is complete and/or the upper surface becomes coated with a graphene layer.

4. Conclusion.

A combination of *in situ* and *ex situ* studies of carbon nanotube growth on a metallic micro-heater show the predicted abrupt transition from multi-walled growth to single-walled growth as the growth temperature is increased. The growth temperatures for the local heating method investigated here are in very good agreement with the growth temperatures required for equivalent products in macroscopic CVD growth. The results shed some light on the growth mechanisms and are in very good qualitative agreement with a model suggested by Wood et al. [24].

The metallic heater undergoes irreversible changes on exposure to the hydrocarbon gas at elevated temperatures. We show that the metallic electrode can become coated with graphene and we interpret the observed rapid increase in resistivity after a carbon-flux dependent incubation time to be due to the formation of molybdenum carbide.

References

1. Englander, O., D. Christensen, and L.W. Lin, *Local synthesis of silicon nanowires and carbon nanotubes on microbridges.* Applied Physics Letters, 2003. **82**(26): p. 4797-4799.
2. Dittmer, S., O.A. Nerushev, and E.E.B. Campbell, *Low ambient temperature CVD growth of carbon nanotubes.* Applied Physics a-Materials Science & Processing, 2006. **84**(3): p. 243-246.
3. Xu, T., et al., *Local synthesis of aligned carbon nanotube bundle arrays by using integrated micro-heaters for interconnect applications.* Nanotechnology, 2009. **20**(29): p. 295303.
4. Lin, W.-C., et al., *Selective local synthesis of nanowires on a microreactor chip.* Sensors and Actuators A: Physical, 2006. **130–131**(0): p. 625-632.
5. Haque, M.S., et al., *On-chip deposition of carbon nanotubes using CMOS microhotplates.* Nanotechnology, 2008. **19**(2): p. 025607.
6. Zhang, K., et al., *Local and CMOS-compatible synthesis of CuO nanowires on a suspended microheater on a silicon substrate.* Nanotechnology, 2010. **21**(23): p. 235602.
7. Mølhave, K., et al., *Epitaxial Integration of Nanowires in Microsystems by Local Micrometer-Scale Vapor-Phase Epitaxy.* Small, 2008. **4**(10): p. 1741-1746.
8. Dittmer, S., et al., *Local heating method for growth of aligned carbon nanotubes at low ambient temperature.* Low Temperature Physics, 2008. **34**(10): p. 834-837.
9. Dittmer, S., et al., *In situ Raman studies of single-walled carbon nanotubes grown by local catalyst heating.* Chemical Physics Letters, 2008. **457**(1-3): p. 206-210.
10. Engstrøm, D.S., et al., *Vertically aligned CNT growth on a microfabricated silicon heater with integrated temperature control—determination of the activation energy from a continuous thermal gradient.* Journal of Micromechanics and Microengineering, 2011. **21**(1): p. 015004.
11. Kawano, T., et al., *Formation and characterization of silicon/carbon nanotube/silicon heterojunctions by local synthesis and assembly.* Applied Physics Letters, 2006. **89**(16): p. 163510.
12. Ek-Weis, J., O.A. Nerushev, and E.E.B. Campbell, *Optical in situ characterisation of carbon nanotube growth.* International Journal of Nanotechnology, 2012. **9**(1-2): p. 3-17.
13. Makita, Y., et al., *Synthesis of single wall carbon nanotubes by using arc discharge technique in nitrogen atmosphere.* European Physical Journal D, 2005. **34**(1-3): p. 287-289.
14. Puretzky, A.A., et al., *In situ measurements and modeling of carbon nanotube array growth kinetics during chemical vapor deposition.* Applied Physics a-Materials Science & Processing, 2005. **81**(2): p. 223-240.
15. Chiashi, S., et al., *Cold wall CVD generation of single-walled carbon nanotubes and in situ Raman scattering measurements of the growth stage.* Chemical Physics Letters, 2004. **386**(1-3): p. 89-94.
16. Kaminska, K., et al., *Real-time in situ Raman imaging of carbon nanotube growth.* Nanotechnology, 2007. **18**(16).

17. de los Arcos, T., et al., *Influence of iron-silicon interaction on the growth of carbon nanotubes produced by chemical vapor deposition.* Applied Physics Letters, 2002. **80**(13): p. 2383-2385.
18. Voelskow, K., et al., *The influence of kinetics, mass transfer and catalyst deactivation on the growth rate of multiwalled carbon nanotubes from ethene on a cobalt-based catalyst.* Chemical Engineering Journal, 2014. **244**: p. 68-74.
19. Sunden, E.O., et al., *Room-temperature chemical vapor deposition and mass detection on a heated atomic force microscope cantilever.* Applied Physics Letters, 2006. **88**(3).
20. Bell, M.S., et al., *Carbon nanotubes by plasma-enhanced chemical vapor deposition.* Pure and Applied Chemistry, 2006. **78**(6): p. 1117-1125.
21. Joensson, M., O.A. Nerushev, and E.E.B. Campbell, *Dc plasma-enhanced chemical vapour deposition growth of carbon nanotubes and nanofibres: in situ spectroscopy and plasma current dependence.* Applied Physics a-Materials Science & Processing, 2007. **88**(2): p. 261-267.
22. Li-Pook-Than, A., J. Lefebvre, and P. Finnie, *Phases of Carbon Nanotube Growth and Population Evolution from in Situ Raman Spectroscopy during Chemical Vapor Deposition.* Journal of Physical Chemistry C, 2010. **114**(25): p. 11018-11025.
23. Harutyunyan, A.R., et al., *Hidden features of the catalyst nanoparticles favorable for single-walled carbon nanotube growth.* Applied Physics Letters, 2007. **90**(16).
24. Wood, R.F., Pannala, S., Wells, J.C., Puretzky, A.A., Geohegan, D.B., *Simple model of the interrelation between single- and multiwall carbon nanotube growth rates*
for the CVD process. Phys. Rev. B, 2007. **75**: p. 253446.
25. Ding, F., Rosen, A., Campbell, E.E.B., Falk, L.K.L., Bolton, K., *Graphitic encapsulation of catalyst particles in carbon nanotube production.* J. Phys. Chem. B, 2006. **110**: p. 7666-7670.
26. Jourdain, V. and C. Bichara, *Current understanding of the growth of carbon nanotubes in catalytic chemical vapour deposition.* Carbon, 2013. **58**: p. 2-39.
27. Geohegan, D.B., et al., *Flux-Dependent Growth Kinetics and Diameter Selectivity in Single-Wall Carbon Nanotube Arrays.* Acs Nano, 2011. **5**(10): p. 8311-8321.
28. Cervantes-Sodi, F., et al., *Viscous State Effect on the Activity of Fe Nanocatalysts.* Acs Nano, 2010. **4**(11): p. 6950-6956.
29. Kobayashi, Y., et al., *Extremely intense Raman signals from single-walled carbon nanotubes suspended between Si nanopillars.* Chemical Physics Letters, 2004. **386**(1-3): p. 153-157.
30. Einarsson, E., et al., *Growth dynamics of vertically aligned single-walled carbon nanotubes from in situ measurements.* Carbon, 2008. **46**(6): p. 923-930.
31. Nerushev, O.A., et al., *Particle size dependence and model for iron-catalyzed growth of carbon nanotubes by thermal chemical vapor deposition.* Journal of Applied Physics, 2003. **93**(7): p. 4185-4190.
32. Yao, Y., et al., □□□□□□□ *Synthesis of carbon nanotube films by thermal CVD in the presence of supported catalyst particles. Part II: the nanotube film. J*. Mat. Sci.: Materials in Electronics, 2004. 15**:** p. 583-594.
33. Picher, M., et al., Se*lf-Deactivation of Single-Walled Carbon Nanotube Growth Studied by in Situ Raman Measurements. N*ano Letters, 2009. 9(**2**): p. 542-547.

34. Futaba, D.N., et al., Ki*netics of Water-Assisted Single-Walled Carbon Nanotube Synthesis Revealed by a Time-Evolution Analysis. P*hysical Review Letters, 2005. 95**(5)**: p. 056104.
35. Zou, Z.Y., et al., Ca*rbide-Forming Groups IVB-VIB Metals: A New Territory in the Periodic Table for CVD Growth of Graphene. N*ano Letters, 2014. 14**(7)**: p. 3832-3839.